Electronic Supplementary Material (ESI) for Dalton Transactions.
This journal is © The Royal Society of Chemistry 2023

Supporting Information for
Elastic and bright assembly-induced luminescent crystal of platinum(II) complexes with near-unity emission quantum yield

Yusuke Makino,[a] Masaki Yoshida,*[ab] Shotaro Hayashi,[c] Toshiyuki Sasaki,[d] Satoshi Takamizawa,[d] Atsushi Kobayashi [a] and Masako Kato*[ab]

[a] Department of Chemistry, Faculty of Science, Hokkaido University
North-10 West-8, Kita-ku, Sapporo, Hokkaido 060-0810, Japan.
[b] Department of Applied Chemistry for Environment, School of Biological and Environmental Sciences, Kwansei Gakuin University
1 Gakuen-Uegahara, Sanda, Hyogo 669-1330, Japan.
[c] School of Environmental Science and Engineering and Research Centre for Molecular Design, Kochi University of Technology
185 Miyanokuchi, Tosayamada, Kami, Kochi 782-8502, Japan.
[d] Department of Materials System Science, Yokohama City University
22-2 Seto, Kanazawa-ku, Yokohama, Kanagawa 236-0027, Japan.

E-mail: masaki.yoshida@kwansei.ac.jp, katom@kwansei.ac.jp

Table of Contents

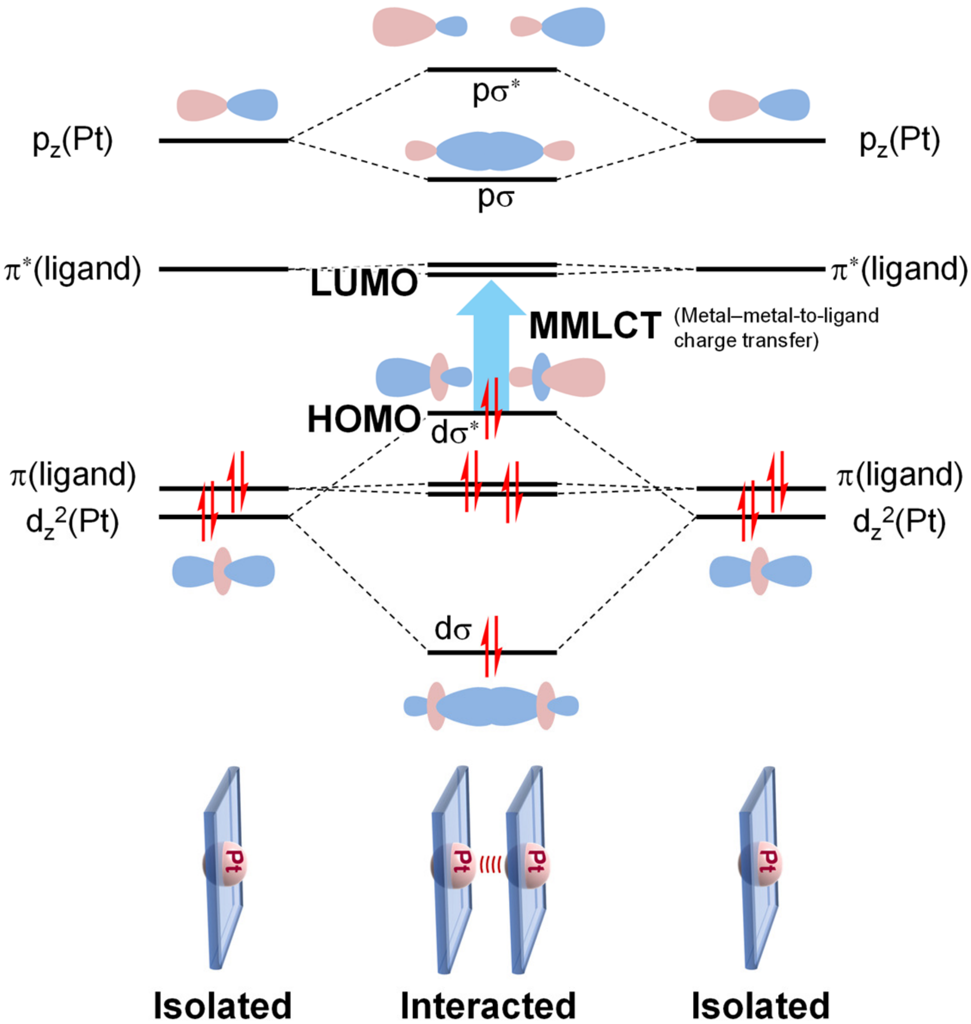

Scheme S1 Schematic MO energy level diagram for Pt(II) complexes with appropriate aromatic ligands showing effective Pt···Pt interaction by stacking. The blue arrow indicates the metal–metal-to-ligand charge transfer (MMLCT) transition.

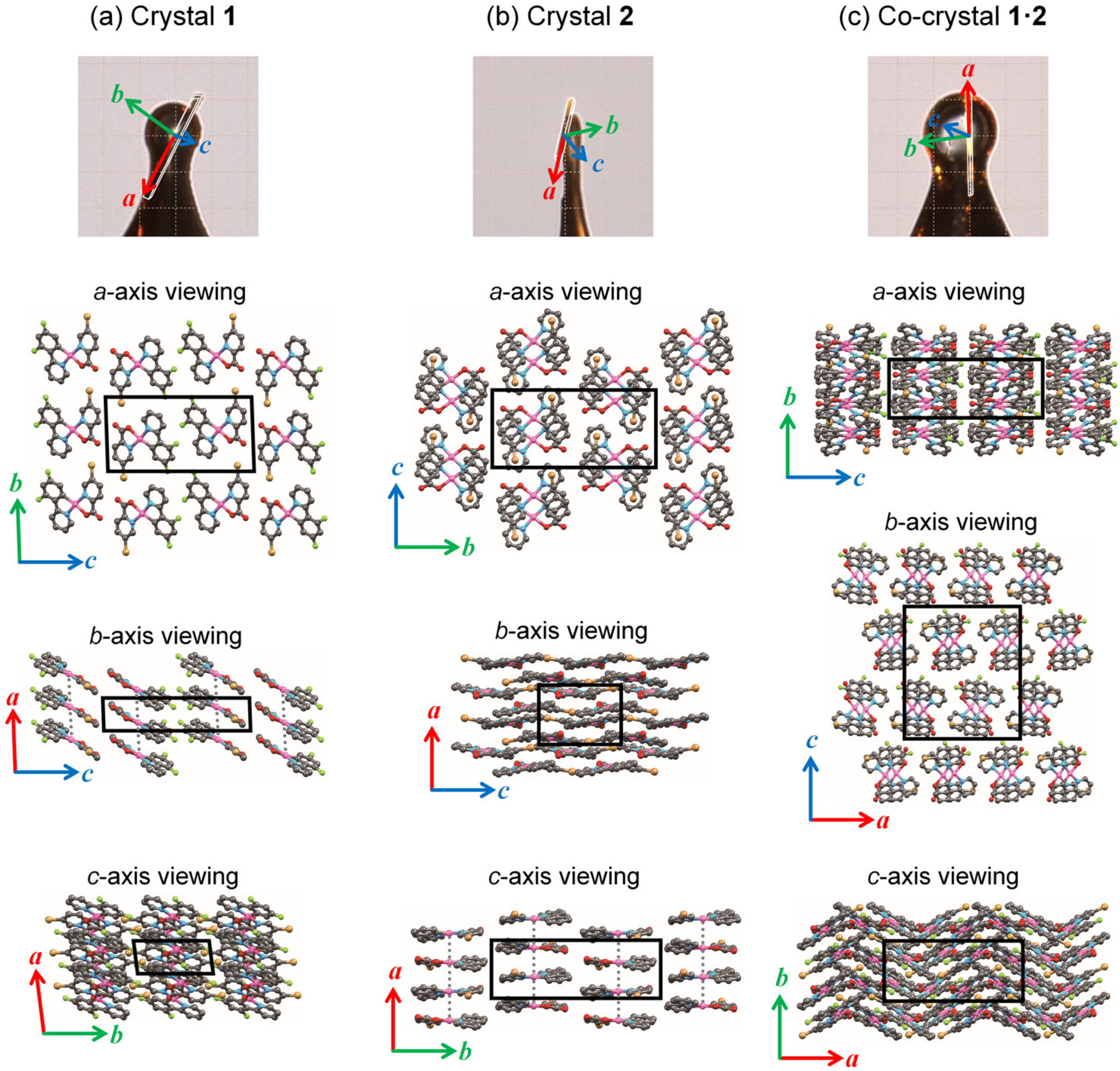

Fig. S1 Crystal photos and packing structures of crystals (a) **1**, (b) **2**, and (c) co-crystal **1·2**. Grey dotted lines in (a) and (b) indicate the Pt···Pt stacking axes.

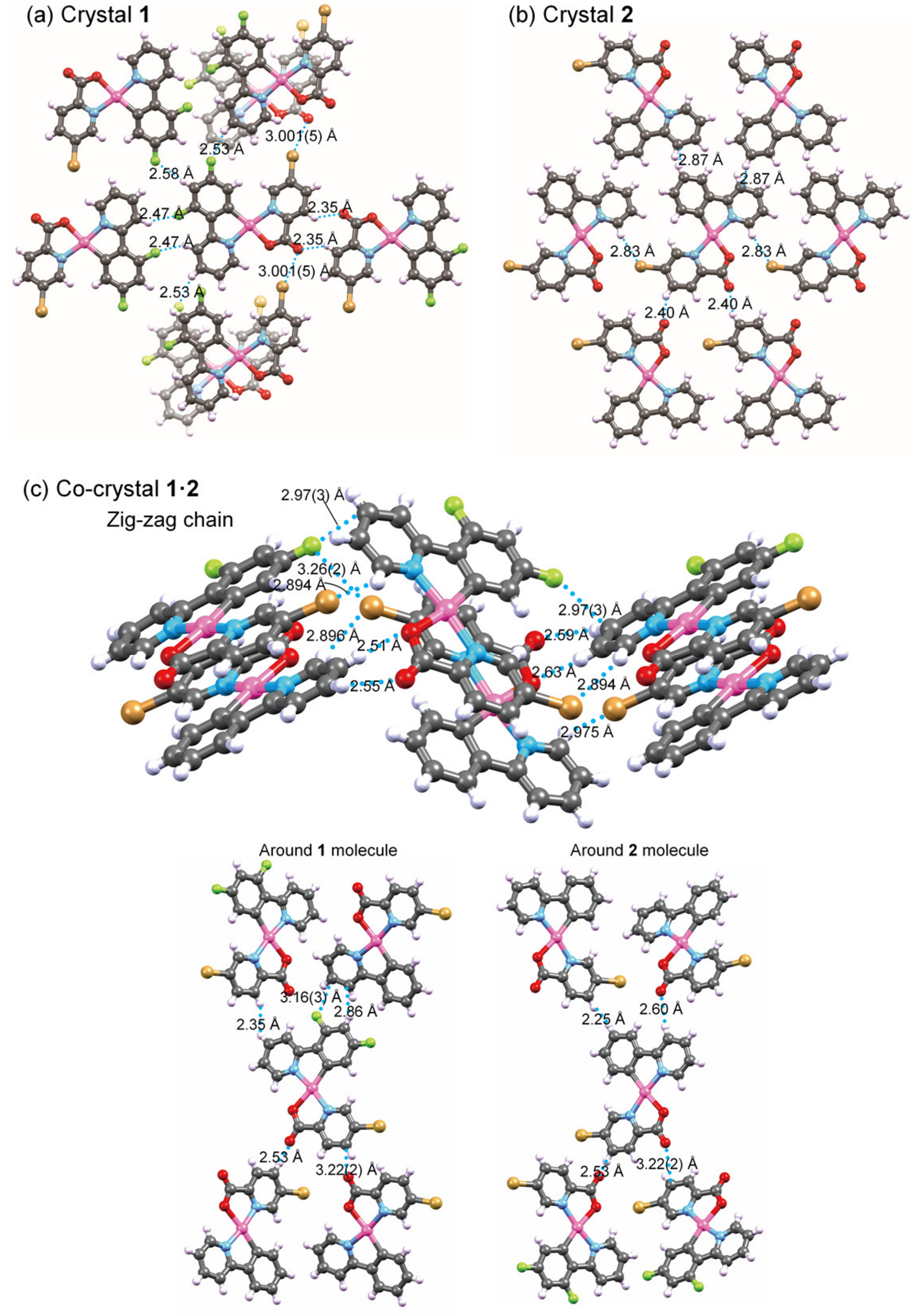

Fig. S2 Intermolecular hydrogen-bonds, halogen interactions, and halogen-π interactions in (a) crystals **1**, (b) **2**, and (c) co-crystal **1**·**2**.

(a)

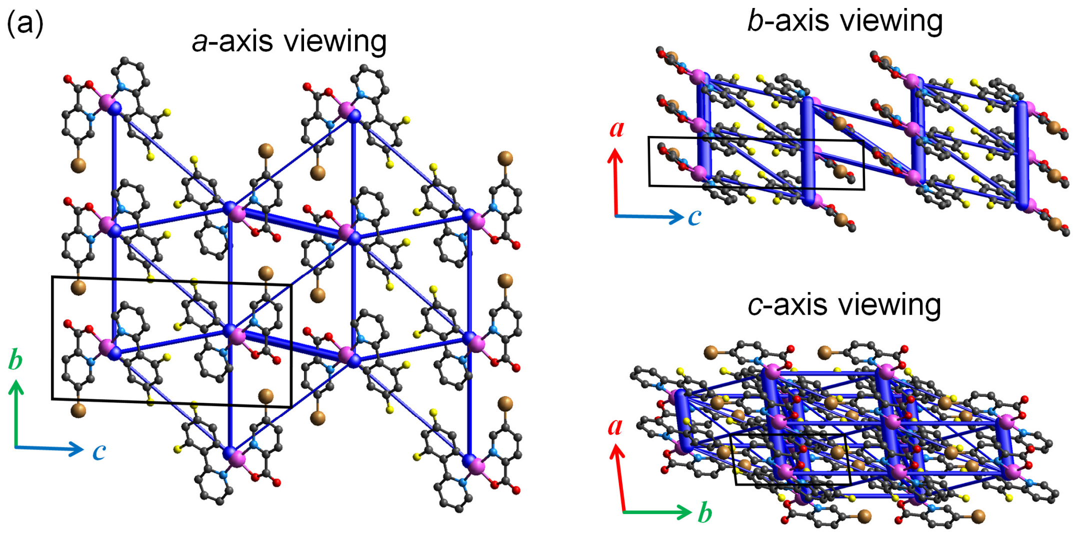

(b)

Interaction Energies (kJ/mol)
R is the distance between molecular centroids (mean atomic position) in Å.

Total energies, only reported for two benchmarked energy models, are the sum of the four energy components, scaled appropriately (see the scale factor table below)

	N	Symop	R	Electron Density	E_ele	E_pol	E_dis	E_rep	E_tot
	2	x, y, z	4.26	B3LYP/DGDZVP	−38.5	−4.3	−125.8	106.2	−87.8
	1	−x, −y, −z	12.73	B3LYP/DGDZVP	−4.0	−1.1	−10.0	0.0	−13.7
	1	−x, −y, −z	11.12	B3LYP/DGDZVP	−50.4	−13.6	−15.3	38.4	−53.0
	2	x, y, z	11.02	B3LYP/DGDZVP	−7.2	−1.4	−13.3	10.8	−13.5
	2	x, y, z	9.64	B3LYP/DGDZVP	−21.8	−6.0	−20.8	32.4	−25.5
	1	−x, −y, −z	10.89	B3LYP/DGDZVP	−8.3	−0.7	−28.6	20.3	−21.7
	1	−x, −y, −z	10.97	B3LYP/DGDZVP	−7.9	−0.5	−16.8	19.4	−11.3
	1	−x, −y, −z	9.60	B3LYP/DGDZVP	−18.5	−8.3	−19.2	19.2	−30.6
	1	−x, −y, −z	12.09	B3LYP/DGDZVP	−8.8	−0.9	−9.4	0.0	−18.2
	1	−x, −y, −z	12.83	B3LYP/DGDZVP	−10.7	−1.1	−14.0	0.0	−24.3

Scale factors for benchmarked energy models
See Mackenzie et al. IUCrJ (2017)

Energy Model	k_ele	k_pol	k_disp	k_rep
CE-HF ... HF/3-21G electron densities	1.019	0.651	0.901	0.811
CE-B3LYP ... B3LYP/6-31G(d,p) electron densities	1.057	0.740	0.871	0.618

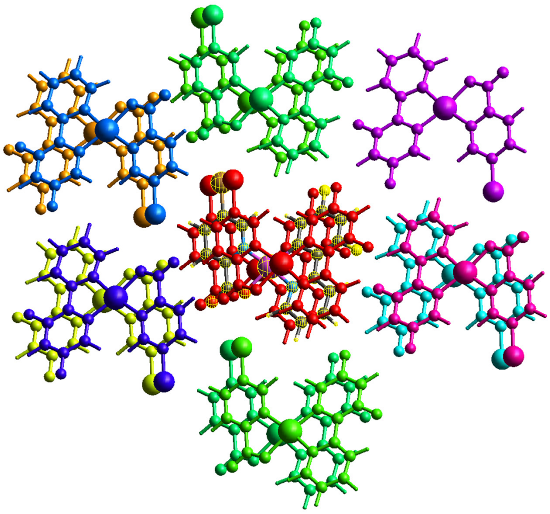

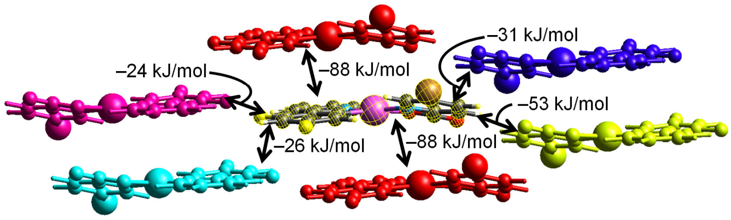

Fig. S3 (a) Energy frameworks of crystal **1’** in total interaction strengths. (b) The interaction energies of various molecular dimers estimated using the CE-B3LYP method. The total energy (E_tot), and electrostatic (E_ele), polarisation (E_pol), dispersion (E_dis), and exchange-repulsion (E_rep) components are listed in the table in the figure.

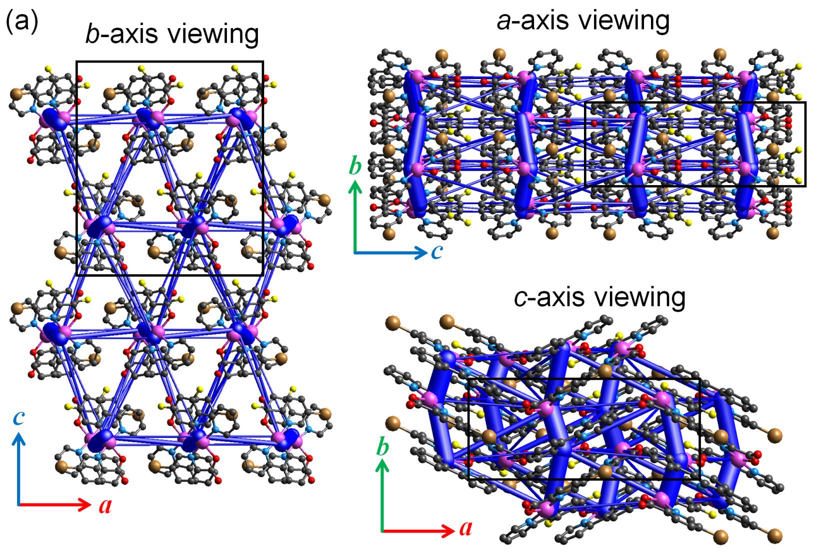

(b)

Interaction Energies (kJ/mol)
R is the distance between molecular centroids (mean atomic position) in Å.

Total energies, only reported for two benchmarked energy models, are the sum of the four energy components, scaled appropriately (see the scale factor table below)

	N	Symop	R	Electron Density	E_ele	E_pol	E_dis	E_rep	E_tot
	1	-	4.09	B3LYP/DGDZVP	−66.4	−6.1	−150.6	152.0	−112.0
	2	−x, −y, z+1/2	11.73	B3LYP/DGDZVP	−3.5	−1.5	−13.9	11.6	−9.8
	1	-	11.61	B3LYP/DGDZVP	−5.5	−1.4	−20.0	19.3	−12.3
	2	x+1/2, −y+1/2, z	9.05	B3LYP/DGDZVP	−9.3	−3.0	−22.3	27.8	−14.3
	1	-	9.77	B3LYP/DGDZVP	−2.4	−0.2	−8.1	5.7	−6.3
	1	-	3.81	B3LYP/DGDZVP	−54.3	−4.1	−120.5	116.4	−93.4
	1	-	9.72	B3LYP/DGDZVP	−2.3	−0.3	−8.0	5.1	−6.5
	1	-	10.75	B3LYP/DGDZVP	−9.0	−5.6	−13.5	11.8	−18.2
	2	−x+1/2, y+1/2, z+1/2	12.15	B3LYP/DGDZVP	−2.5	−4.0	−12.6	0.0	−16.6
	1	-	10.02	B3LYP/DGDZVP	−23.9	−5.9	−16.5	16.3	−34.0
	1	-	11.86	B3LYP/DGDZVP	−4.0	−0.4	−11.5	6.3	−10.6
	1	-	9.98	B3LYP/DGDZVP	−26.5	−6.5	−17.0	21.0	−34.7
	1	-	11.02	B3LYP/DGDZVP	−14.6	−5.3	−8.7	12.6	−19.2
	0	−x+1/2, y+1/2, z+1/2	12.04	B3LYP/DGDZVP	−6.6	−1.3	−13.9	0.0	−20.1
	0	x+1/2, −y+1/2, z	9.05	B3LYP/DGDZVP	−4.0	−3.4	−19.0	17.1	−12.7
	0	−x, −y, z+1/2	11.92	B3LYP/DGDZVP	−12.1	−5.3	−10.1	9.0	−20.0

Scale factors for benchmarked energy models
See Mackenzie et al. IUCrJ (2017)

Energy Model	k_ele	k_pol	k_disp	k_rep
CE-HF ... HF/3-21G electron densities	1.019	0.651	0.901	0.811
CE-B3LYP ... B3LYP/6-31G(d,p) electron densities	1.057	0.740	0.871	0.618

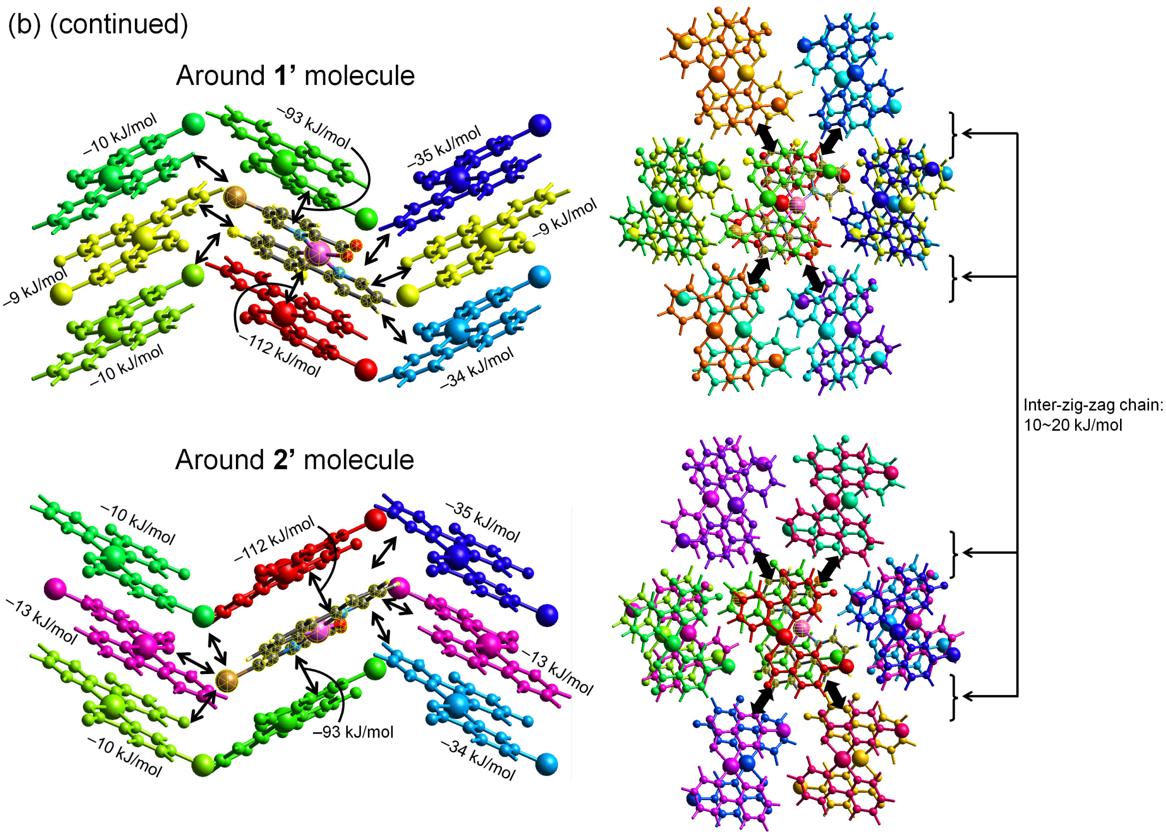

Fig. S4 (a) Energy frameworks of co-crystal **1'·2'** in total interaction strengths. (b) The interaction energies of various molecular dimers estimated using the CE-B3LYP method. The total energy (E_tot), and electrostatic (E_ele), polarisation (E_pol), dispersion (E_dis), and exchange-repulsion (E_rep) components are listed in the table in the figure.

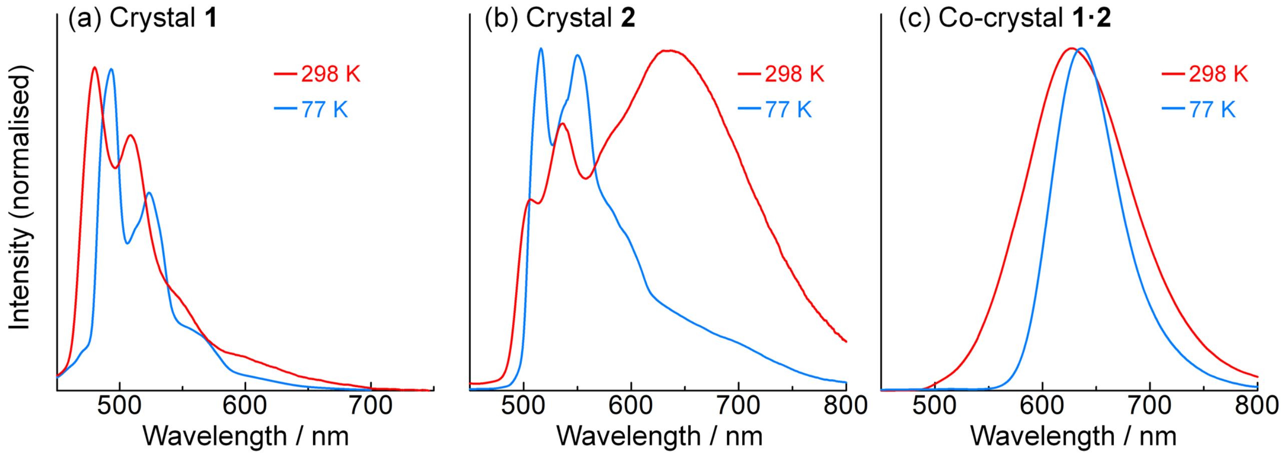

Fig. S5 Emission spectra of crystals (a) **1**, (b) **2**, and (c) co-crystal **1·2** (λ_{ex} = 350 nm) at 298 K (red line) and 77 K (blue line).

In the case of **2**, only the structured emission band assignable to the $^3\pi\pi^*$ emission was observed at 77 K, where the broad emission band at around 600 nm disappeared. Therefore this lower-energy emission band of **2** at 298 K can be attributed to the excimer-derived emission due to the excited state structural deformation. The excitation spectrum of **2** at 298 K (Fig. S6(b)) and the emission decay profile of **2** (Fig. S7(b)) also supported this assignment.

For co-crystal **1·2**, the emission band was only slightly red-shifted at 77 K (628 → 637 nm). The ^{3}MMLCT emission of Pt(II) complexes is known to red-shift significantly at low temperatures depending on the delocalisation of the excited state,[S1] but in the present co-crystal **1·2**, the metallophilic interaction is only effective between two molecules, so no change in the delocalisation should have occurred. Thus, the shift in luminescence is considered to be small even at 77 K.

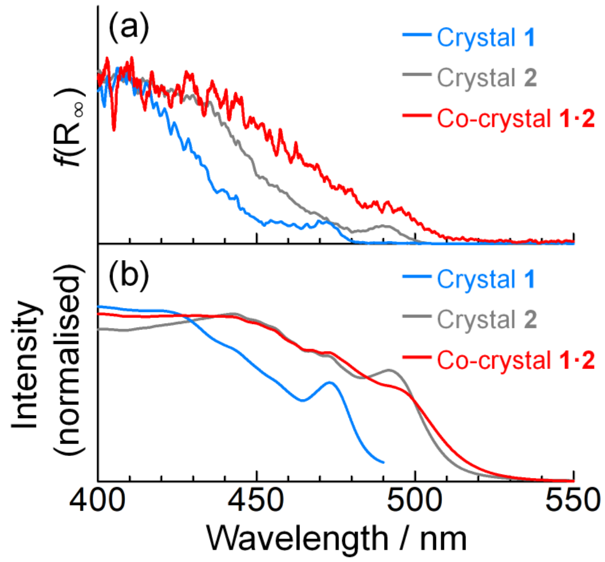

Fig. S6 (a) UV-vis diffuse-reflectance and (b) excitation spectra of crystals **1** (blue line), **2** (grey line), and co-crystal **1·2** (red line) at 298 K. The detection wavelengths for the excitation spectra were 480 nm (for **1**), 630 nm (for **2**; detected by the excimer-derived emission band), and 628 nm (for **1·2**).

For **1** and **2**, the sharp absorption/excitation bands originating from the spin-forbidden $^3\pi\pi^*$ transition were observed at the lowest energy side in both diffuse-reflectance and excitation spectra. Importantly, even though the excitation spectrum for crystal **2** is detected in the lower energy side of the emission band (630 nm), the spin-forbidden $^3\pi\pi^*$ absorption was observed in the excitation spectrum. This indicated the negligible Pt···Pt interaction between the molecules of complex **2** in the ground state, and thus the lower energy emission band should be attributed to the structural deformation during the excitation.

In contrast to **1** and **2**, the spectra of **1·2** have a new shoulder on the lower energy side, attributed to the ^{3}MMLCT transition originating from the Pt···Pt interaction. This assignment was further supported by the TDDFT calculation (Fig. S8(b)).

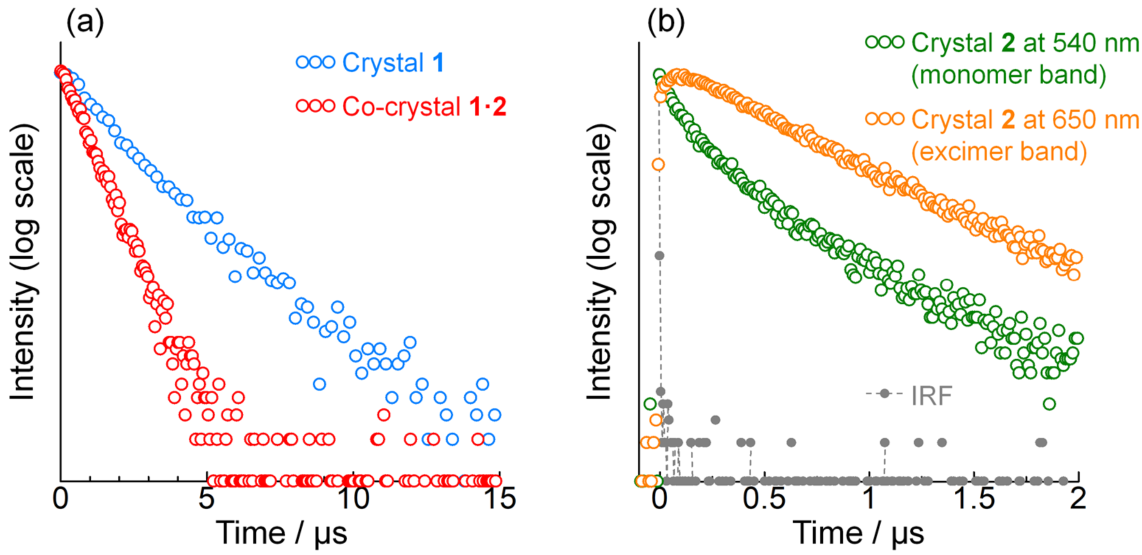

Fig. S7 Emission decays of (a) crystal **1** (blue) and co-crystal **1·2** (red), and (b) crystal **2** detected at 540 nm (green) and 650 nm (orange) at 298 K (λ_{ex} = 340 nm). The grey dashed line in (b) shows the instrument response function (IRF).

The emission decay of co-crystal **1·2** was analysed with single component decay (τ = 828 ns), whereas that of **1** was analysed with two components of similar values (τ_1 = 1.54 μs (A_1 = 0.83), τ_2 = 3.42 μs (A_2 = 0.17), τ_{av} = 2.13 μs; A_i are the pre-exponential factors for τ_i). The emission decay of **2** at 540 nm (assignable to the monomer emission band) was also analysed with two components (τ_1 = 113 ns (A_1 = 0.66), τ_2 = 413 ns (A_2 = 0.34), τ_{av} = 310 ns). On the other hand, the emission decay profile of **2** at 650 nm (longer-wavelength emission band) clearly showed the fast rise ($\tau_{1(rise)}$ = 54.6 ns ($A_{1(rise)}$ = –1.53)) prior to the single component decay ($\tau_{2(decay)}$ = 471 ns ($A_{2(decay)}$ = 2.53)). Thus, we have concluded that the longer-wavelength emission band of **2** should be assignable to the excimer emission band.

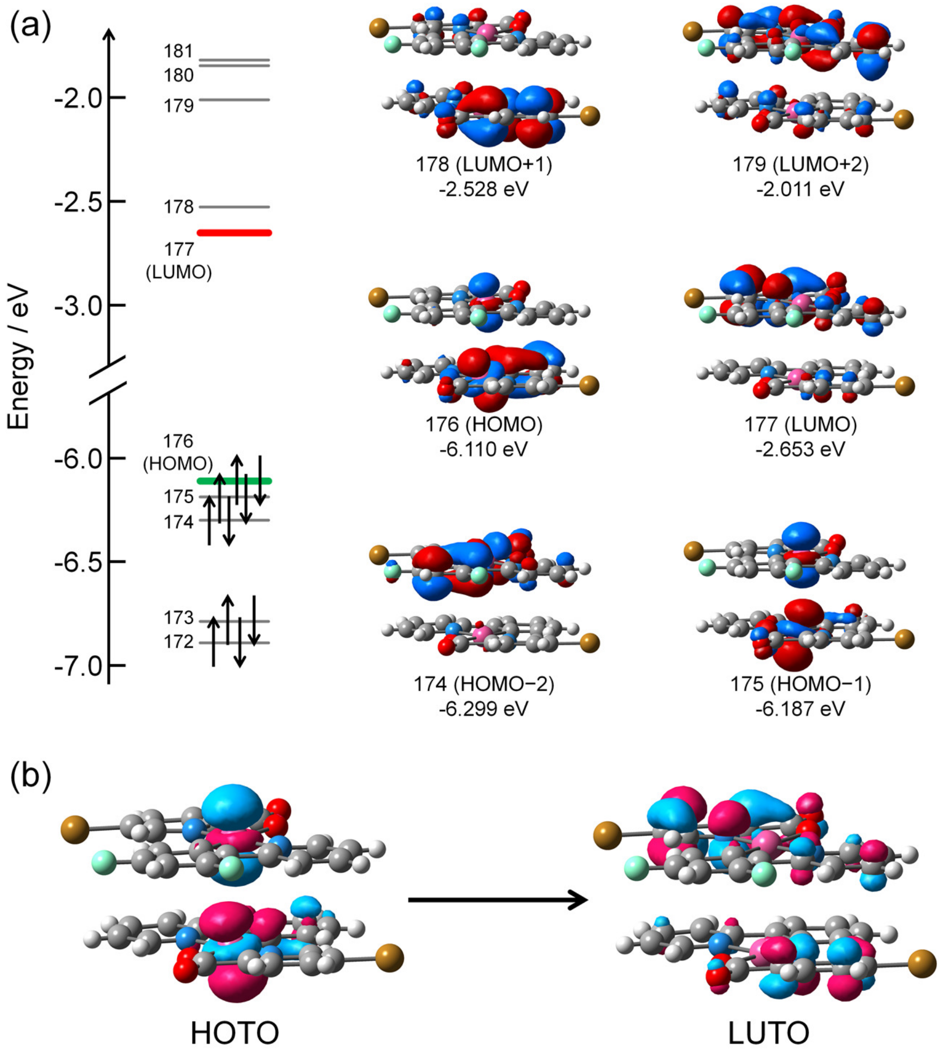

Fig. S8 (a) Kohn-Sham orbitals at the frontier region of the dimeric unit of co-crystal **1·2** (isovalue = 0.035). HOMO and HOMO−1 are mainly localised on the dσ* orbital between two Pt atoms (besides, HOMO is also slightly localised on the ligands), while LUMO to LUMO+2 are delocalised on the π* orbitals of the ligands. (b) Natural transition orbitals (NTOs) of the dimeric unit of co-crystal **1·2** for the 1st vertical excitation (λ = 475.75 nm, *f* = 0.0131). The highest occupied transition orbital (HOTO) and the lowest unoccupied transition orbital (LUTO) indicate the occupied "hole" and the unoccupied "electron", respectively. This result suggests that the lowest excited state of **1·2** could be assignable to the dσ*→π* transition, i.e., MMLCT transition.

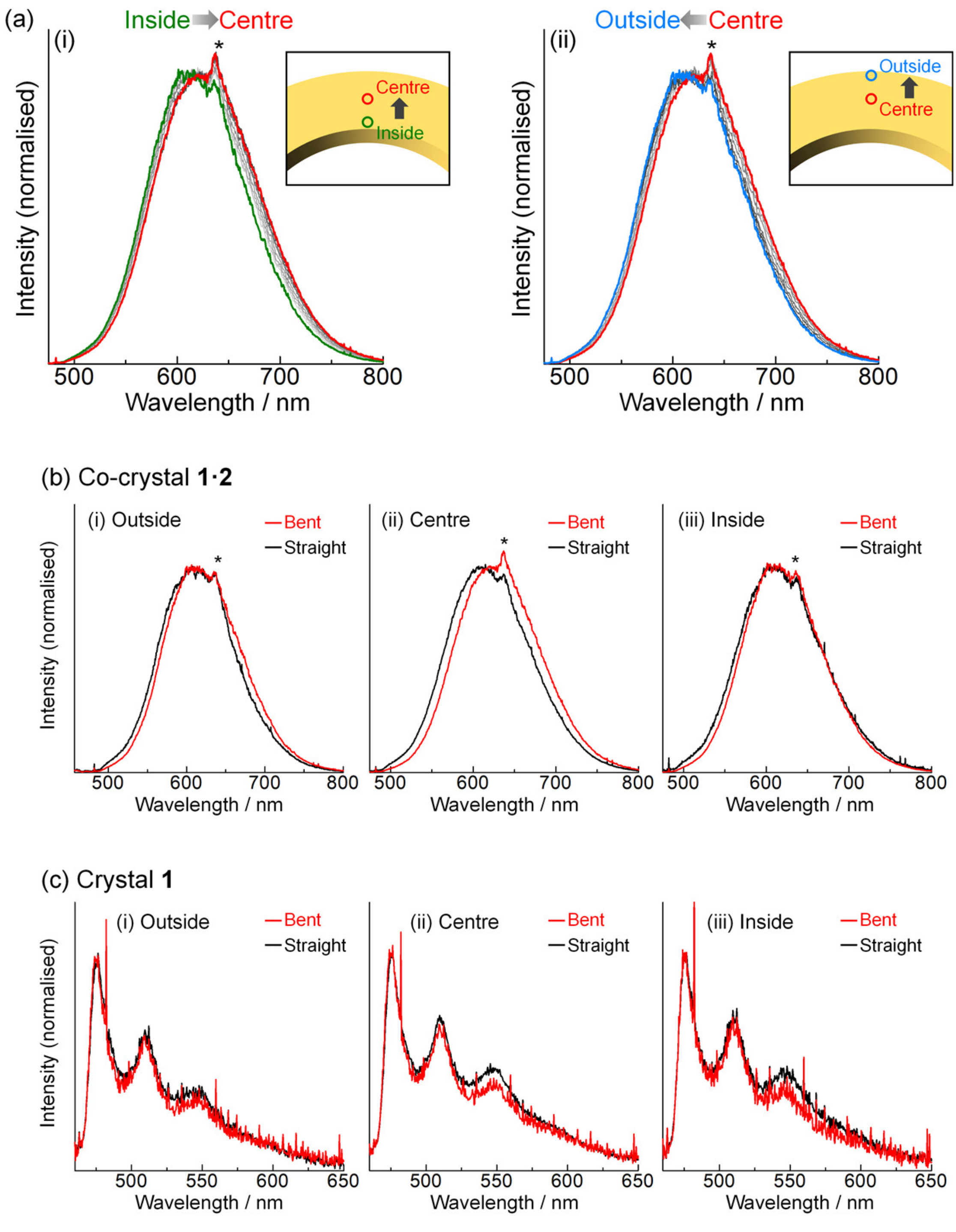

Fig. S9 Spatially resolved microscopic photoluminescence (μPL) spectra (λ_{ex} = 405 nm; ca. 500 × 500 nm for each measurement area) for (a,b) co-crystal **1·2** (ε_a = 0.8%) and (c) crystal **1** (ε_a = 2.3%). The peak indicated with an asterisk (*) is an artifact from the spectrometer. (a) The emission spectra for the bent co-crystal **1·2** showed (i) a gradual red-shift from the inside to the centre of the bent crystal, and (ii) a gradual blue-shift from the centre to the outside. (b,c) Emission spectra at the (i) outside, (ii) centre, and (iii) inside positions of the bent (red line) and straight (black line) crystals of the (b) co-crystal **1·2** and the (c) crystal **1**. A shift of the emission maximum due to bending was observed only in the central part of co-crystal **1·2**.

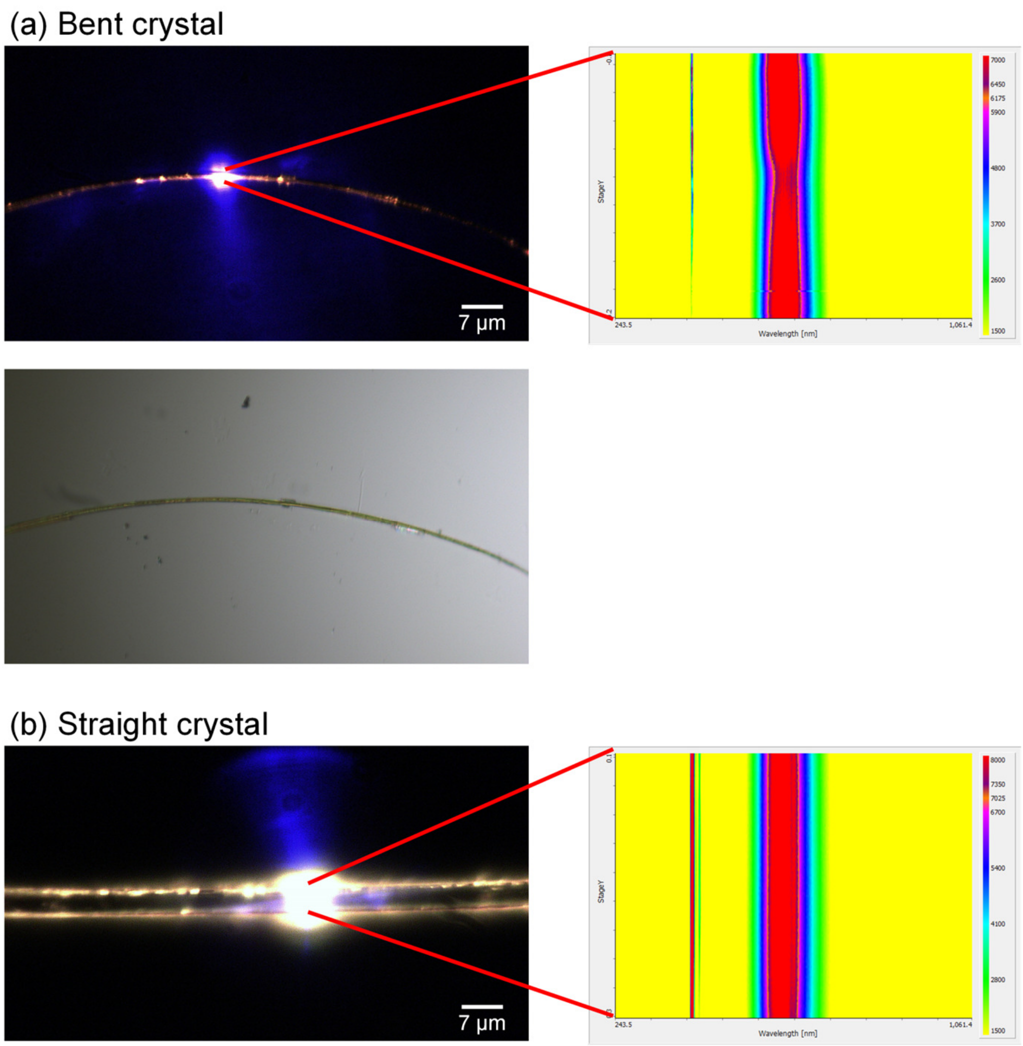

Fig. S10 Spatially resolved photoluminescence mappings for (a) bent (ε_a = 0.4%) and straight crystals of co-crystal **1**·**2**.

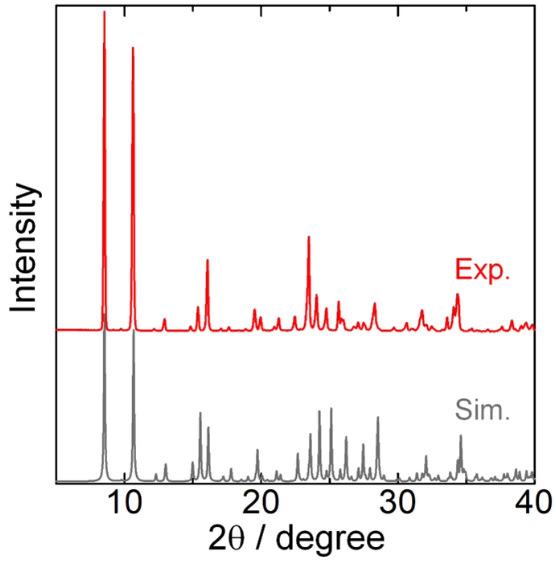

Fig. S11 Powder X-ray diffraction (PXRD) pattern of the polycrystalline sample of co-crystal **1·2** (red line). Grey line indicates the simulated pattern based on the crystal structure of **1·2**. Since the experimental PXRD pattern was almost identical to that of the simulated one, the obtained bulk sample of **1·2** should have the same structure as that obtained from the single crystal X-ray structural analysis (Fig. 1(c)).

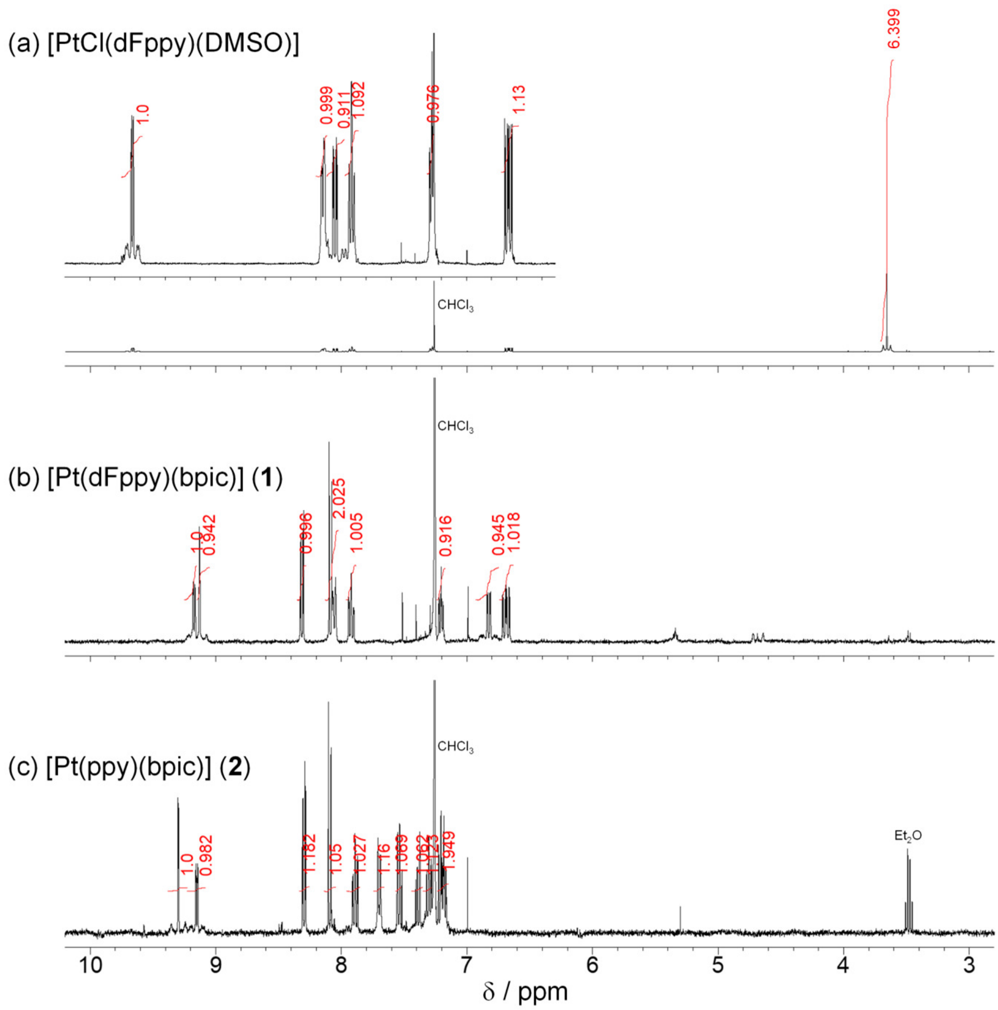

Fig. S12 ^{1}H NMR spectra of present complexes (400 MHz, $CDCl_3$).

The elastic modulus E (Pa) was calculated on a formula (1):[S2]

$$E = \left(\frac{2 f_n \pi l^2}{\lambda_n^2}\right)^2 \frac{\rho A}{I} \qquad (1)$$

where f is resonance frequency (Hz), l is length of a vibrating part of a crystal specimen (m), λ_n are 1.875 (n=1) and 4.694 (n=2), ρ is density (kg m^{-3}), A is cross-sectional area (m^2), and I is sectional moment of inertia (m^4). Sectional moment of inertia for a specimen with a rectangular section is calculated on the following equation (2):

$$I = \frac{bh^3}{12} \qquad (2)$$

where b and h are length of a rectangular section (m) perpendicular and parallel to vibrating direction, respectively.

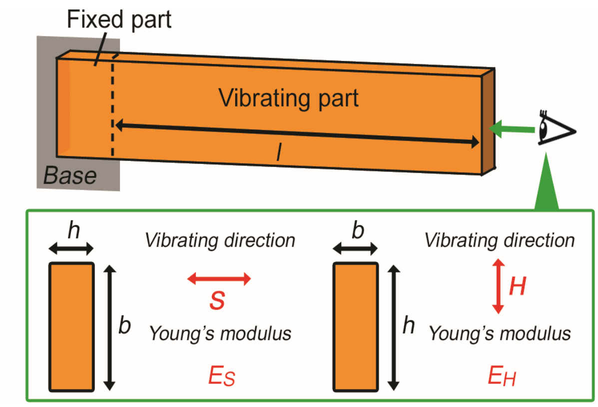

Table S1 Elastic moduli (Young's moduli) and related parameters of **1** and co-crystal **1·2**.

	Vibrating direction	Crystal size / m^3	ρ / kg m^{-3}	f / Hz	E / GPa
1	S (short-axis)	$(778 \times 10^{-6}) \times (19 \times 10^{-6}) \times (11 \times 10^{-6})$	2.577	834	0.21
	H (mid-axis)			3657	1.3
Co-crystal **1·2**	S (short-axis)	$(884 \times 10^{-6}) \times (13 \times 10^{-6}) \times (13 \times 10^{-6})$	2.569	2317	1.9
	H (mid-axis)			2679	2.6

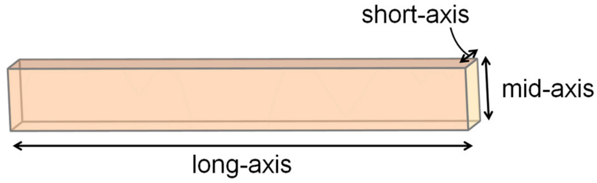

Table S2 Selected interatomic distances (Å) and angles (deg) of **1**, **2**, and co-crystal **1·2**.

	1	**2**	**1** in **1·2**	**2** in **1·2**[a]
		Distances / Å		
Pt1-C1	2.001(7)	1.991(8)	1.98(2)	2.02(2)
Pt1-N1	2.001(6)	1.990(6)	1.995(15)	1.991(13)
Pt1-N2	2.032(6)	2.032(6)	2.043(15)	2.056(16)
Pt1-O1	2.073(5)	2.092(5)	2.082(13)	2.108(15)
Pt1-Pt1	4.2648(4)	4.5265(4)	3.5793(9) and 5.0181(9)	
		Angles / deg		
C1-Pt1-N1	81.3(3)	80.9(3)	80.3(7)	82.1(7)
C1-Pt1-N2	105.8(3)	105.7(3)	107.5(7)	106.0(7)
C1-Pt1-O1	171.8(2)	173.1(3)	171.6(7)	173.6(7)
N1-Pt1-N2	172.3(2)	171.3(3)	172.2(6)	171.9(7)
N1-Pt1-O1	93.1(2)	94.1(2)	91.6(6)	91.8(6)
N2-Pt1-O1	80.2(2)	79.8(2)	80.7(6)	80.1(6)

[a] Pt2, C18, N3, N4, and O3 atoms in **2** in **1·2** correspond to Pt1, C1, N1, N2, and O1 atoms in **1** in **1·2**.

Supplementary Tables for X-ray crystallography and DFT calculation

Table S3 Crystal parameters and refinement data.

	1	**2**	Co-crystal **1·2**
Formula	$C_{17}H_9BrF_2N_2O_2Pt$	$C_{17}H_{11}BrN_2O_2Pt$	$C_{17}H_9BrF_2N_2O_2Pt$ • $C_{17}H_{11}BrN_2O_2Pt$
Formula weight	586.26	550.28	1136.54
Crystal system	Triclinic	Orthorhombic	Orthorhombic
Space group	$P\bar{1}$ (#2)	$P2_12_12_1$ (#19)	$Pna2_1$ (#33)
a / Å	4.2648(2)	7.1788(1)	18.1002(6)
b / Å	9.6408(4)	20.8576(4)	7.8365(2)
c / Å	18.7288(7)	9.8686(2)	20.7171(5)
α / deg	91.577(3)	90	90
β / deg	91.691(4)	90	90
γ / deg	97.222(4)	90	90
V / Å^3	763.23(6)	1477.65(5)	2938.6(1)
Z	2	4	4
D_{calc} / g cm^{-1}	2.551	2.474	2.569
T / K	150	150	150
Reflns collected	7903	5744	9769
Unique reflns	3077	2670	4618
GOF on F^2	1.087	1.063	1.067
R_{int}	0.0459	0.0250	0.0410
R_1 ($I > 2\sigma(I)$)[a]	0.0370	0.0235	0.0455
wR_2[b]	0.1083	0.0628	0.1199
CCDC No.	2225408	2225409	2225410

[a] $R_1 = \Sigma||F_o|-|F_c|| / \Sigma|F_o|$. [b] $wR_2 = [\Sigma w(F_o^2 - F_c^2) / \Sigma w(F_o)^2]^{1/2}$, $w = [\sigma_c^2(F_o^2) + (xP)^2 + yP]^{-1}$, $P = (F_o^2 - 2F_c^2)/3$.

Table S4 Computed vertical excitations of the dimeric unit of co-crystal **1·2**.

Excited State 1:	Singlet-A	2.6061 eV	475.75 nm	*f*=0.0131	<S**2>=0.000
175 -> 177	0.38672				
176 -> 177	0.54813				
176 -> 178	0.16689				
Excited State 2:	Singlet-A	2.6635 eV	465.49 nm	*f*=0.0122	<S**2>=0.000
175 -> 177	-0.39716				
175 -> 178	-0.33601				
176 -> 177	0.18426				
176 -> 178	0.42369				
Excited State 3:	Singlet-A	2.7055 eV	458.27 nm	*f*=0.0008	<S**2>=0.000
174 -> 177	-0.12228				
175 -> 178	0.50949				
176 -> 177	-0.14504				
176 -> 178	0.42715				
Excited State 4:	Singlet-A	2.7422 eV	452.14 nm	*f*=0.0059	<S**2>=0.000
174 -> 177	0.64817				
174 -> 178	-0.11005				
176 -> 177	-0.15358				
176 -> 178	0.15686				
Excited State 5:	Singlet-A	2.8288 eV	438.29 nm	*f*=0.0010	<S**2>=0.000
174 -> 177	-0.16280				
175 -> 177	0.42046				
175 -> 178	-0.33278				
176 -> 177	-0.33552				
176 -> 178	0.25673				
Excited State 6:	Singlet-A	3.0425 eV	407.51 nm	*f*=0.0029	<S**2>=0.000
174 -> 177	0.12638				
174 -> 178	0.68724				
Excited State 7:	Singlet-A	3.1941 eV	388.17 nm	*f*=0.0097	<S**2>=0.000
175 -> 179	0.40179				

(Continued)

176 -> 179	0.51295				
176 -> 181	-0.17998				
Excited State 8:	Singlet-A	3.2650 eV	379.74 nm	*f*=0.0062	<S**2>=0.000
175 -> 179	0.43103				
175 -> 181	-0.18249				
176 -> 179	-0.22792				
176 -> 180	-0.32242				
176 -> 181	0.31503				
Excited State 9:	Singlet-A	3.3145 eV	374.07 nm	*f*=0.0014	<S**2>=0.000
174 -> 179	0.17924				
175 -> 179	0.11212				
175 -> 180	0.41080				
175 -> 181	-0.30934				
176 -> 179	-0.16348				
176 -> 180	0.31514				
176 -> 181	-0.16839				
Excited State 10:	Singlet-A	3.3437 eV	370.80 nm	*f*=0.0064	<S**2>=0.000
173 -> 177	-0.18305				
174 -> 179	0.53858				
174 -> 180	-0.28303				
175 -> 180	-0.20237				
175 -> 181	0.16315				

References.

S1 M. Nakagaki, S. Aono, M. Kato and S. Sakaki, *J. Phys. Chem. C*, 2020, **124**, 10453.

S2 (a) M. Horio and S. Onogi, *J. Appl. Phys.*, 1951, **22**, 977; (b) D. R. Bland and E. H. Lee, *J. Appl. Phys.*, 1955, **26**, 1497; (c) K. Hashimoto, M. Sakane, M. Ohnami and T. Yoshida, *J. Soc. Mater. Sci., Jpn.*, 1995, **44**, 1456; (d) T. Sasaki, S. Sakamoto, K. Nishizawa and S. Takamizawa, *Cryst. Growth Des.*, 2020, **20**, 3913.